Journal of Clinical Laser Medicine & Surgery
Volume 18, Number 3, 2000
Mary Ann Liebert, Inc.
Pp. 117–123

A Comparison of Cunyite and Fosterite NIR Tunable Laser Tissue Welding Using Native Collagen Fluorescence Imaging

JING TANG, M.D., Ph.D.,[1] FANAN ZENG, B.S.,[1] JONATHAN M. EVANS, Ph.D.,[1] BING XU, Ph.D.,[1] HOWARD SAVAGE, Ph.D.,[2] PENG PEI HO, Ph.D.,[1] and R.R. ALFANO, Ph.D.[1]

ABSTRACT

Objective: **To evaluate the technique of native collagen fluorescence imaging for assessing the extent of welded areas for tissues exposed to different near-infrared (NIR) laser wavelengths.** ***Background:*** **Native fluorescence imaging may be used to identify the distribution of collagen and elastin in tissues. Our past work demonstrated that different welding strengths were obtained under the same laser power conditions using different NIR wavelengths. The role of collagen in tissue welding experiments is not well understood.** ***Methods:*** **Two new NIR tunable lasers were used to weld canine skin. The welded areas on the surface and in cross sections were analyzed by measuring the spatial distribution of native collagen fluorescence at 380 nm excited by 340 nm radiation.** ***Results:*** **The results show that native collagen fluorescence imaging is a useful technique for analyzing the extent of tissue welds produced under a range of laser exposures. Fluorescence imaging reveals the depth of laser interaction with the tissue as well as evaluating collateral damage to the tissue surface. The welded volume obtained in skin using Cunyite laser exposure at 1,430 nm is deeper than that produced with Forsterite laser exposure at 1,250 nm. The post welded tensile strength for the same power density is greater for the Cunyite lasers. Ablated tissue on the surface is more prevalent with Forsterite laser welding at 1,250 nm than with Cunyite at 1,430 nm.** ***Conclusion:*** **Native collagen fluorescence can distinguish between tissue welds that have been produced by different NIR wavelengths. Tissue welding using 1,430nm radiation is more effective than that using 1,250nm.**

INTRODUCTION

Fluorescence spectroscopy allows the measurement of electronic transitions of various chromophores in the complex tissue structure. There are several natural fluorophores that exist in tissue which, when excited with ultraviolet light, fluoresce in the ultraviolet and visible regions of the spectrum. Collagen is an important photoactive molecule in tissue.[1] Native fluorescence imaging of an intrinsic molecule or tissue component in the sample may be performed with different selected emission and excitation wavelengths. In our recent study,[2] native fluorescence imaging was performed on the cross section of tissue that had been exposed to intense laser radiation. The collagen emission wavelength (λ_c) of 380 nm was monitored for an excitation wavelength (λ_e) of 340 nm. The laser exposed region was clearly revealed, due to collagen denaturation by laser irradiation and the subsequent loss of its native fluorescence. Collagen fluorescence imaging offers a novel way to easily detect *in situ* the distribution and quantitative changes in collagen.

In this paper, we report on the use of native collagen fluorescence imaging to assess the extent of collagen denaturation in a region of tissue that has been repaired using the laser tissue welding (LTW) technique.

LTW can be achieved by directing a low-energy laser beam of appropriate wavelength at the edges of the tissue cut.[3] Laser surgery has been reported to have many advantages over conventional suture techniques, such as less foreign body reaction, more rapid healing, less constriction, and reduced surgical time.[4–7] Although success has been achieved in experimental and clinical applications of laser welding, there remain several

[1]Institute for Ultrafast Spectroscopy and Lasers and New York State Center for Advanced Technology for Ultrafast Photonic Materials and Applications, Departments of Physics and Electrical Engineering, The City College and Graduate School of the City University of New York, New York, New York.
[2]Department of Pathology, New York Eye and Ear Infirmary, New York, New York.

key areas in which the procedure can be improved to extend its usage in the medical field. Previous studies indicate that the bursting strengths of laser-assisted blood vessel anastomoses are reduced compared to conventional suture repair.[8,9] Aneurysm formation has been reported to be in the 6–29% range[8,10,11] for laser welding procedures. To improve the tensile strength of laser-repaired tissue, some authors reported that the addition of some protein solders, such as albumin[12,13] and fibrin[14,15] has enhanced the laser-welded tissue strength. Thermal damage to tissue surrounding the welded volume can be reduced through the use of photoactive dyes. Dyes such as indocyanine green[16] and fluorescein isothiocyanate (FITC)[17,18] have been used to localize the light absorption to the desired tissue region, thereby eliminating unwanted secondary tissue injury. These modifications in the laser welding technique are not without their drawbacks; for instance, the use of protein solders increases the likelihood of contamination and viral infection and dyes are possibly toxic and carcinogenic. Our approach to laser welding using tunable lasers in the 1,200- to 1,500-nm wavelength range offers the ability to form strong tissue bonds without introducing potentially harmful foreign elements.[19]

Our previous laser welding study without the use of an additive or foreign agent demonstrated that different welding results are obtained with the same laser conditions but using different near-infrared (NIR) wavelengths. Our results show that a greater water absorption wavelength is correlated to a higher tensile strength of the laser-welded tissue. Tunable NIR lasers, such as, Cr:forsterite,[20] tunable from 1,150 to 1,350 nm, and Cunyite ($Cr:Ca_2GeO_4$),[21] tunable from 1,350 to 1,500 nm, can be used for tissue welding based on absorption of water and native chromophores in tissue. The selection of particular NIR wavelengths can improve welding and avoid thermal injury to tissue. LTW may be possible using the absorption bands of water in the 1,150- to 1,500-nm spectral region without additional proteins or dyes. An attractive feature Cr^{4+} lasers for LTW is that they offer more versatility in selecting precise depth penetration. The tuning range of Cr^{4+} lasers overlaps a region of varying water absorption; this property may be used advantageously. The tissue depth to which the laser light is effective for the welding process is governed by the strength of the tissue absorption that is dominated by water in this wavelength region. By tuning the laser wavelength, a continuous range of penetration depths may be accessed depending on the effective water absorption.

The objective of this study is to evaluate the technique of native collagen fluorescence imaging for comparing welding regions generated with Cunyite and Forsterite lasers at different wavelengths. This work will help to elucidate the effect of native tissue water absorption on the weld depth and ultimate bond strength.

MATERIALS AND METHODS

Cunyite and Forsterite lasers provide continuous beams of tunable NIR radiation. The emission wavelength of the Cunyite laser was tuned from 1,350 to 1,500 nm with a maximal power output of 320 mW at 1,430 nm. The emission wavelength of the Forsterite laser was tuned from 1,130 to 1,370 nm with a maximal power output of 450 mW at 1,250 nm.

The laser welding setup is shown in Fig. 1. The beam was delivered in a noncontact manner. It was focused with a short focal length lens (f = 70 mm) producing a spot size of 0.4 mm, positioned at 50 mm from the lens. The wavelength was measured with a spectrometer (Rees, Instruments, Godalming, UK). The power out of the focus lens was measured with a power meter (Scientech 372, Boulder, CO). The laser wavelengths, which were selected for the tissue welding, were dependent on the maximal power output of these two laser prototypes: 1,430 nm for the Cunyite tunable laser, and 1,250 nm for the Forsterite. For the Cunyite tunable laser, the power was 220 mW. The power density was 175 W/cm^2. For the Forsterite tunable LTW, the power was kept at 400 mW from the out-of-focus lens. The power density was 318 W/cm^2. With these laser conditions, the highest tensile strengths were achieved for skin welding using these two lasers. The details on the use of this critique method to detect the tensile strength were described in our previous work.[19]

The canine skin sample was harvested atraumatically from animals being etherized from another study that did not involve the skin tissue. The institutional animal review board approved the use of available animal tissue (Protocol No. 8803). After shaving the fur, a cut was made of size 5 × 5 mm. Two skin pieces were placed border to border on a translation stage. Laser welding was performed between two skin pieces with scanning laser irradiation. The stage was moved forward at approximately 5 mm/30 sec, then back at the same speed and for the same length. A 5-mm fusion line was performed. No conventional suture was performed. The total exposure time was one minute. The energy fluence was 10.5 kJ/cm^2 for Cunyite tunable laser welding, and 19.1 kJ/cm^2 for Forsterite.

After LTW was performed, the surfaces of the skin samples were mounted on a quartz slide for native collagen fluorescence imaging as well as back-illuminated photography. Then, the samples were kept at −20°C for 15 min. While the sample was frozen, a cross-section (*X-Z* plane, see Fig. 2a) through the center of the welded line and perpendicular to the *X-Y* plane was selected for imaging the welded region. The fluorescence imaging and daylight back-illuminated photography were performed on the cut cross-section of the joint region of the sample on the *X-Z* surface (Fig. 2a).

A schematic diagram of the native collagen fluorescence imaging setup is shown in Fig. 2b. The excitation light beam

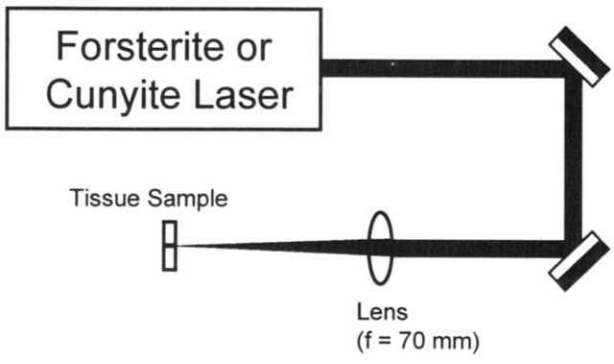

FIG. 1. Forsterite and Cunyite laser setup for tissue welding.

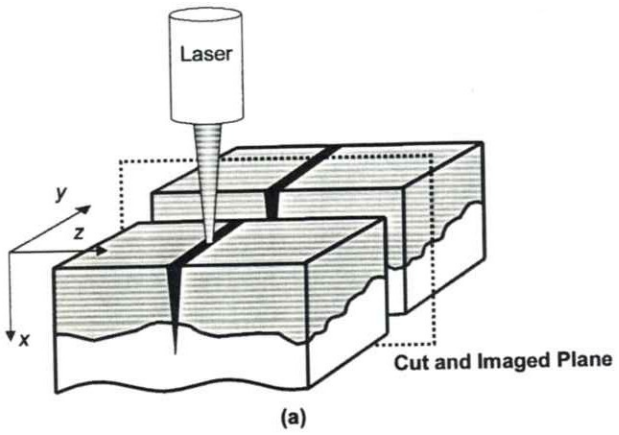

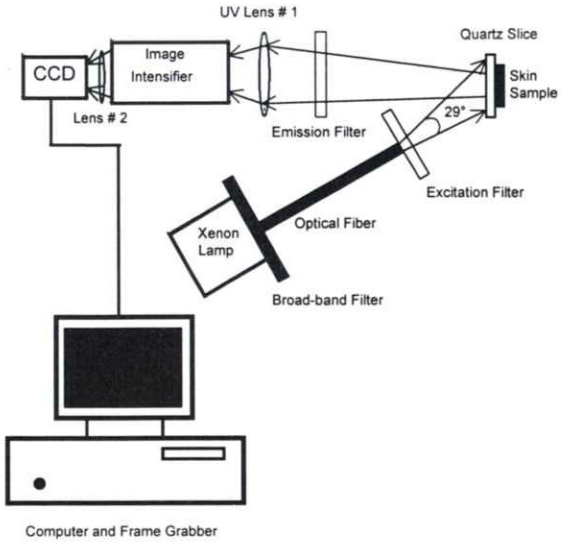

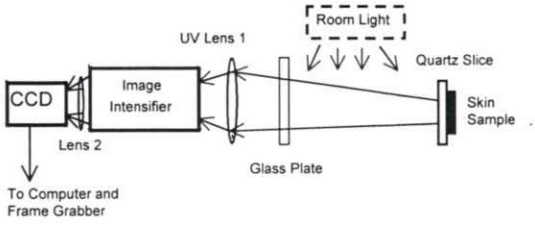

FIG. 2. (**a**) Repaired skin sample in cross section for fluorescence imaging. Laser beam xirradiates the skin (*Z-Y* plane) surface for tissue welding. The cross section (*X-Z* plane) through the center of the welded line and perpendicular to the *X-Y* plane is the imaged (*X-Z*) cross-section surface. (**b**) Fluorescence imaging setup to probe the tissue weld joint. A light beam from the *Xenon Lamp* is passed through the broad band filter and transmitted by the *Optical Fiber* to excite sample surface. The emitted beam is passed through a narrow-band *Excitation Filter* (340 nm for collagen imaging, and 380 nm for elastin imaging). The fluorescence from the sample is collected by *UV Lens #1* and imaged onto an *Image Intensifier.* The *Emission Filter* at 380 nm selects the collagen signal, and at 450 nm selects the elastin signal and is inserted at the front of the UV Lens #1. The signals are amplified by the image intensifier. The intensified fluorescence image is then imaged by *Lens #2* onto the CCD camera. A personal computer is used to digitize, display, and analyze the image profiles. (**c**) Back-illuminated photography setup. The glass plate is placed at the front of the *UV Lens #1* instead of the emission filter to obtain the same focus and size image as for fluorescence imaging. The sample is illuminated with room daylight.

from a high-intensity xenon lamp (300 W) was sent through a broadband filter to reduce heat and then it was transmitted by an optic fiber (Excitation Fiber). Before exciting the surface of the sample, the light beam was sent through a narrow band filter λ_e = 340 nm (Excitation Filter). The central portion of the 10-nm bandwidth light beam was used to illuminate the sample. The fluorescence from the sample was collected by a 105-mm focal length UV-Nikkor camera lens (Lens #1) in the back-scattering geometry and focused into an image intensifier. A narrowband filter λ_c = 380 nm (Emission Filter) was inserted at the front of the UV camera lens for fluorescence imaging of the sample. After the signal was amplified by the image intensifier, the fluorescence image was re-imaged with a lens (Lens #2) onto a CCD camera (Photometrics CH350, Tucson, AZ). Three pictures per second can be obtained from this imaging system. To improve the signal to noise, each image was averaged over 10 pictures. A personal computer was used to digitize and analyze the image. The controlling software generated and displayed the fluorescence maps.

The setup used for white-light illuminated photography of the joint is shown in Fig. 2c. A glass plate was placed in front of Lens #1 instead of the emission filter to obtain the same focus and image size as in fluorescence imaging. The sample was illuminated with room lights.

After obtaining native fluorescence and white-light imaging, the tissue samples were fixed in 10% phosphate-buffered formalin. The tissues were dehydrated in graded ethanol solution and xylene, and embedded in paraffin. Each of the lesions was sectioned at 5 μm. Sections from the lesion were stained with Gill's hematoxylin eosin, picrosirius red F3BA, and Orcein stains. The specimen stained with picrosirius red F3BA was examined with a polarizing microscope (Reichert, Vienna, Austria) The other specimens were examined with a normal optical microscope (Vanox-T, Olympus, Japan). Both microscopes were equipped with a color video camera with 3 CCD chips (DXC-97 MD, Sony, Japan) for obtaining histology images.

RESULTS

The effect of the Cunyite tunable laser at 1,430 nm on skin welding was observed as a slight discoloration and translucence

at the fusion line with 175 W/cm^2 power density. The average initial post-welded tensile strength value was 0.65 ± 0.12 N (n = 10). In the case of the Forsterite tunable laser at 1,250 nm, no color changes were observed with ≈0 N tensile strength, when the same power density as the Cunyite laser was used. When the power density of the Forsterite laser was increased to 318 W/cm^2, the resultant LTW gave a 0.28 ± 0.10 N tensile strength (n = 10). There was a statistical significance in the average initial post-welded tensile strength between these two groups ($t = 7.223$, $p < 0.01$). In skin welding with the Forsterite tunable laser at 1,250 nm skin welding, a slight tissue ablation in the surface of the welded tissue occurred. The welded site became darkened (Fig. 3a′).

The native collagen fluorescence images and the white-light-illuminated photographs of the welded samples on the surface are shown in Fig. 3. With Cunyite laser welding, the two pieces of skin were completely welded. The welded site was invisible on the white-light photograph (Fig. 3a), but the welded region can be seen as a 0.5-mm-wide black line on the fluorescence image (Fig. 3b), due to reduction of the native collagen fluorescence. With Forsterite laser welding, there was carbonization on the welded tissue surface. A clear black line was seen on the welded site on the white-light photograph (Fig 3a′). This region became a little wider line on the collagen fluorescence image, due to tissue ablation plus loss of native collagen fluorescence (Fig. 3b′).

The cross sections of the native collagen fluorescence images and white-light illuminated photographs of the welded samples are shown in Fig. 4. The welded site was not evident on the photograph after Cunyite laser welding (Fig. 4a). In the native fluorescence image (Fig. 4b), the welded site became a fluorescence void due to the collagen denaturing by laser heating and the consequent loss of fluorescence. The depth of the welded region from the skin surface to the deepest point is 1.7 ± 0.4 mm (n = 10). Forsterite laser welding produced a shallower weld depth of 0.4 ± 0.3 mm (n = 10). The dark region observable on the white-light and fluorescence images (Fig. 4, a′ and b′) is a crater formed on the tissue surface, a result of tissue ablation during the welding procedure (Fig. 4a′). The crater appears deeper in the fluorescence image, in this case the dark region is composed of the ablated crater plus the loss fluorescence associated with the denaturing of the native collagen (Fig. 4b′).

Histology with picrosirius red F3BA stain with and without illumination by polarized light is shown in Fig. 5. Tissue ablation on the skin surface (uppermost) is more evident after Forsterite laser welding (Fig. 5a′) than for Cunyite (Fig. 5a). Under unpolarized illumination, the stained tissue structure at the welded site becomes homogenized. The denatured collagen fibers on the junction cannot be identified without polarized light illumination. Polarized light illumination gives insight into the extent of the denatured collagen in the welded region

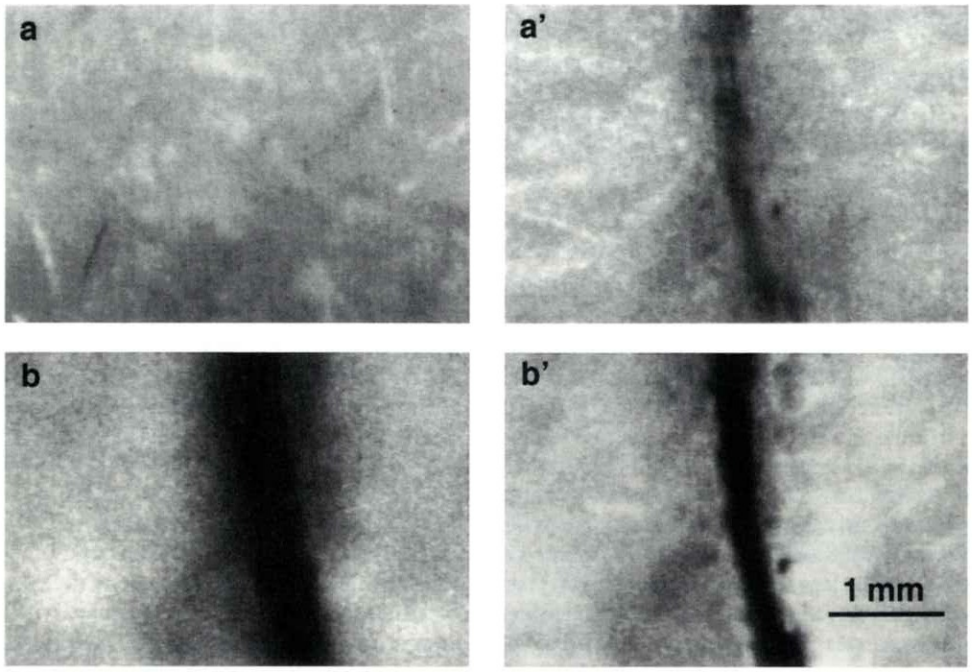

FIG. 3. Surface images of welded skin tissue. (**a**) Cunyite laser at 1,430 nm welding; the two pieces of skin were completely welded. The welded site was invisible on the back-illuminated photograph. (**b**) On the collagen fluorescence image, a 0.5-mm-wide black line was seen due to loss of native collagen fluorescence. (**a′**) Forsterite laser at 1,250 nm welding; there was carbonization in the welded tissue surface. A clear black line was seen on the welded site on the back-illuminated photograph. (**b′**) On the collagen fluorescence image, a little wider line was seen due to the tissue ablation plus a loss of native collagen fluorescence in the surrounding tissue. The boundary between tissue ablation and loss of collagen fluorescence cannot be distinguished in this picture.

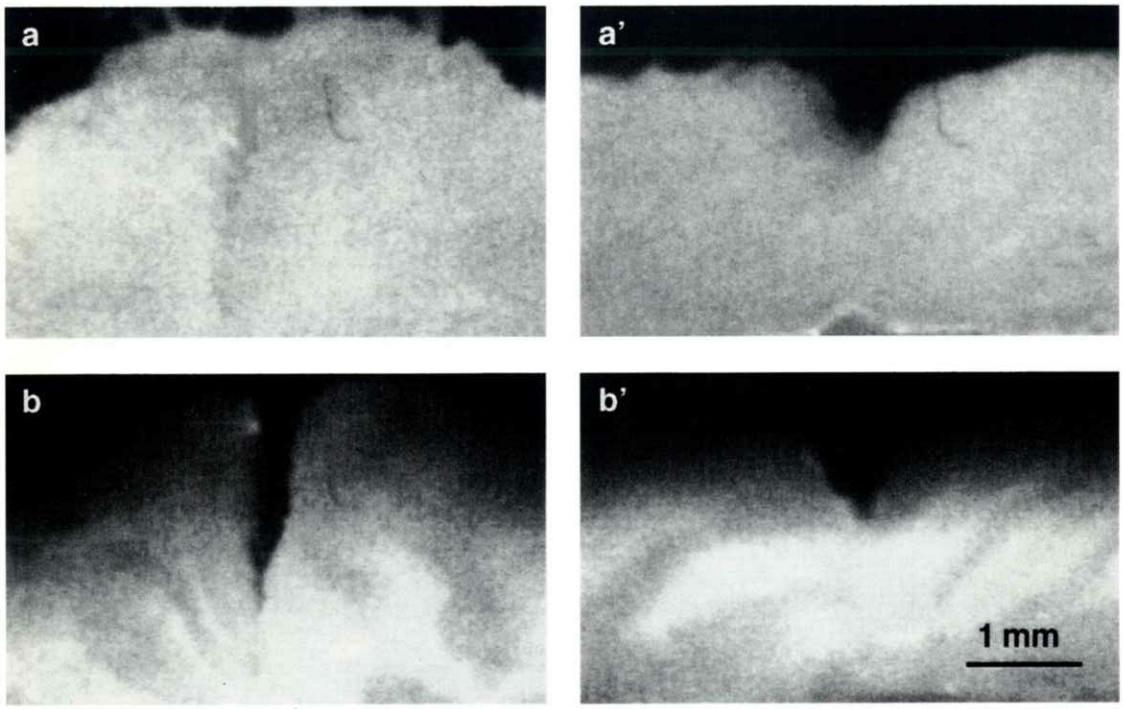

FIG. 4. Cross-section images of welded skin tissue. (**a**) Cunyite laser at 1,430 nm welding; the welded site was not clear on the back illuminated photograph. (**b**) On the collagen fluorescence image, a deep crater is visible on the fluorescence image due to the loss of native collagen fluorescence at the welded site. (**a′**) With Forsterite laser welding, there was a small crater on the surface of sample at the back-illuminated photograph, due to tissue ablation. (**b′**) On the collagen fluorescence image, a slightly bit deeper crater was demonstrated, due to the tissue ablation plus a loss of native collagen fluorescence in the surrounding tissue.

due to the loss of birefringence experienced by collagen in the denaturing process. The crater of the void in collagen birefringence is more apparent after Cunyite laser welding (Fig. 5b) than Forsterite (Fig. 5b′). The crater depth and size in these histological results are quite similar to these in native collagen fluorescence imaging (Fig. 4, b and b′). The difference in the extent of collagen denaturing apparent when comparing Fig. 4b and Fig. 5b is explained by the increased contrast that fluorescence imaging affords between regions of total and partial collagen denaturing. In Fig. 4b, fluorescence from collagen present in the tissue adjacent to the junction is strong despite a partial denaturing of the collagen in this region whereas the total denaturing at the site of the junction is conspicuous by the absence of fluorescence. Although the junction can be observed in the histology data shown in Fig. 5b, it is not so clearly defined as it appears in Fig. 4b. This is because the partially denatured collagen regions adjacent to the junction appear gray in the histology data.

DISCUSSION

The studies reported here were designed to demonstrate the effective localization in welding an area of tissue using the native collagen fluorescence as a noninvasive imaging method. The relationship between water absorption wavelengths and the welded depth, which is of concern in repairing tensile strength after laser welding, is revealed.

It is believed that thermal or photochemical reactions or a combination of the two are involved in LTW.[3] It now seems reasonable to assume that most of the native tissue welding effect of laser light can be attributed to collagen denaturation and binding from the thermal dissipation of the energy in the tissue.[4,22–24] This study with the native collagen fluorescence imaging method confirms that collagen fibers on welded junctions are denatured after laser tissue welding. Because tissues are composed primarily of water,[25] their water absorption characteristics become important in tissue welding. Our observation from previous work suggests that the wavelength dependence of the weld's tensile strength can be related to water absorption wavelengths. The greater water absorption is correlated to the higher tensile strength.[19] These results are obtained from a direct measurement of tensile strength with a digital force gauge after laser skin welding without a morphologic support.

In the present study, a collagen native fluorescence imaging technique is used to visualize the welded area in the tissues welded with different wavelengths. Comparison of the fluorescence images (Fig. 4, b and b′) for the 1,250- and 1,430-nm exposed tissues reveals two obvious differences. First, the effective depth of the welded region is greater for long-wavelength exposure (1,430 nm) to that produced using shorter-wavelength

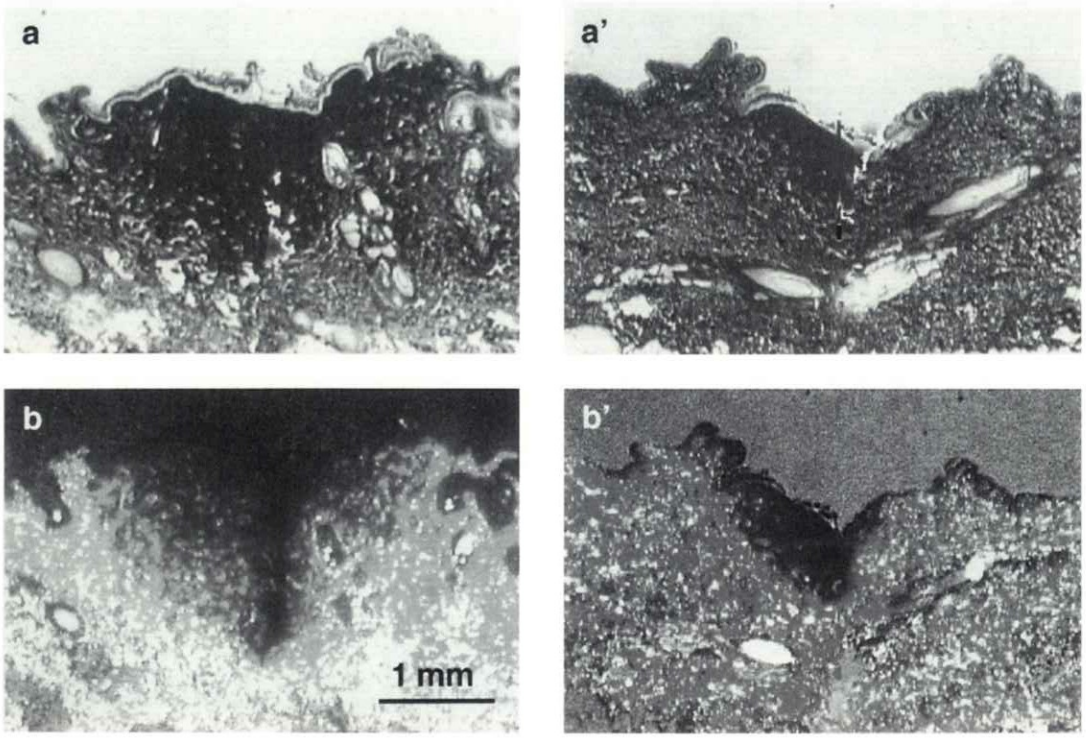

FIG. 5. Histological cross sections of skin tissue after Cunyite (left) and Forsterite (right) tunable laser welding showing the welded joint. Sections (**a**) and (**a′**) are stained using picrosirius red F3BA and viewed without polarized light. The tissue structure at the welded joint becomes homogenized. The denatured collagen fibers in the junction cannot be identified. Under polarized light (sections **b** and **b′**), stained collagen fibers cannot be seen on the welded junction, due to collagen denaturing and the loss of its natural birefringence. The welded junction appears as a crater. Note there is a much deeper crater on the welded area using Cunyite laser welding than that of Forsterite. (Original magnification ×16.)

light (1,250 nm) and, second, the surface damage post-welding due to tissue ablation is more extensive for shorter-wavelength exposure. These results may be explained in terms of the inherent optical properties of the tissue exposed, namely absorption and scatter. In general, longer wavelengths will experience less scattering than shorter wavelengths in the same medium. In our experiment, this results in the longer-wavelength light retaining its focussed beam property deeper into the tissue. This property, together with the enhanced absorption experienced at 1,430 over 1,250 nm, leads to the more efficient transfer of light energy to the tissue to form the tissue bond. This result can well explain why 1,430-nm welding produces a greater tensile strength than for 1,250 nm for canine skin welding in this study. Moreover, 1,250-nm welding needs almost two times more energy than 1,430 nm (19.1 kJ/cm^2 *vs.* 10.5 kJ/cm^2) and causes tissue ablation on the surface of the welded site, which is a harmful effect of LTW.

The Forsterite and Cunyite tunable lasers emit radiation in the NIR desired spectral range, where there is less scattering and deeper penetration than for visible light lasers,[26] such as Argon (1 to 2 mm) and other lasers, such as Nd:YAG lasers (3 to 4 mm)[27] and the middle infrared CO_2 laser (0.02 mm).[28] These Cr^{4+}-based laser beams have penetration depths varying from 2 to 5 mm, depending on the wavelength. Water and adipose in the tissue can maximally absorb laser energy to heat and induce binding from collagen and elastin. These Cr^{4+}-based lasers may be suitable for both thin-wall tissues, such as small blood vessel anastomoses, as well as for thicker-wall tissue welds, such as skin, digestive tubes, and the urinary system, when the appropriate wavelength is chosen. The two lasers can be tuned to various wavelengths from 1,150 to 1,500 nm to adjust the welded depths. Output of these lasers has several key advantages over single-wavelength lasers.[26] The irradiation can be tuned to the absorption bands of different tissue constituents, such as the 1,203-nm band for adipose and the 1,350-nm band for water. In addition, their second harmonic output (575–750 nm) can be turned to the hemoglobin band in blood vessels.[28,29] Different kinds of tissues can be welded by selecting different NIR wavelengths. An additional advantage in the use of these lasers is using quartz fiber optics to deliver the beams, which a surgeon can easily operate.

We have shown that native collagen fluorescence imaging is a valuable tool for evaluating the effectiveness of the LTW technique under different operating conditions. In the future, a truly noninvasive method of generating depth information on collagen denaturing below the tissue surface is envisioned by using a two-photon excitation technique to generate collagen fluorescence.

ACKNOWLEDGMENTS

This work is supported by the DOE Center of Excellence Program. We thank Dr. N. Ockman for proofreading and suggestions. We thank Columbia Presbyterian Hospital for the supply of canine skin samples.

REFERENCES

1. Alfano, R.R., and Katz, A. (1996). Photonic pathology, fluorescence and Raman spectroscopy for tissue diagnosis and characterization, Analytical Use of Fluorescent Probes in Oncology. New York: Plenum Press, pp. 81–89.
2. Tang, J., Zeng, F.A., Ho, P.P., and Alfano, R.R. (2000). Fluorescence spectroscopic imaging to detect changes in collagen and elastin following laser tissue welding. Submitted to J Clin Laser Med. Surg 18, 3–8.
3. Guthrie, C.R., Murray, L.M., Kopchok, G.E., Rosengaum, D., and White, R.A. (1991). Biochemical mechanism of laser vascular tissue fusion. J. Invest. Surg. 4, 3–12.
4. Bass, L.S. (1995). Laser tissue welding: A comprehensive review of current and future clinical applications. Lasers Surg. Med. 17, 315–349.
5. Poppas, D.P., Choma, T.J., Rooke, C.T., Klioze, S.D. and Schlossberg, S.M. (1993). Preparation of human albumin solder for laser tissue welding. Lasers Surg. Med. 13, 577–580.
6. Tang, J., Godlewski, G., Rouy, S., Dauzat, M., Juan, J.M., Chambettaz, F., Delacretaz, G., and Salathe, R.P. (1994). Microarterial anastomosis using a non contact diode laser versus a control study. Lasers Surg. Med. 14, 229–237.
7. Tang, J., Godlewski, G., Rouy, S., Prudhomme, M., Delacretaz, G., and Salathe, R.P. (1997). Morphological analysis of the microaterial media repair after 830 nm diode laser assisted end-to-end anastomosis, comparison with conventional manual suture. Laser Med. Sci. 12, 300–308.
8. Quigley, M.R., Bailes, J.E., and Kwaan, H.C. (1985). Comparison of bursting strength between suture and laser-anastmosed vessel. Microsurgery 6, 229–232.
9. Basu, S., Wang, S., and Robertazzi, R. (1988). In vitro bursting strength studies of laser welding tissue and comparison with conventional anastomosis. J. Vasc. Surg. 7, 420–422.
10. Pribil, S., and Powers, S.K. (1985) Carotid artery end-to-end anastomosis in the rat using the argon laser. J. Neurosurg. 63, 771–775.
11. Vale, B.H., Frenkel, A., and Trenka-Benthin, S. (1986). Microsurgical anastomosis of rat carotid arteries with CO_2 laser. Plast. Recrnstr. Surg. 77, 759–763.
12. Wright, E.J., and Poppas, D.P. (1997). Effect of laser wavelength and protein solder concentration on acute tissue repair using laser welding: initial results in a canine ureter model. Techn. Urol. 3, 176–181.
13. Poppas, D.P., Choma, T.J., Rooke, C.T., Klioze, S.D., and Schlossberg, S.M. (1993). Preparation of human albumin solder for laser tissue welding. Lasers Surg. Med. 13, 577–580.
14. Grubbs, P.E., Wang, S., Marini, C., Basu, S., Rose, D.M., and Cunningham, J.N. (1988). Enhancement of CO_2 laser system with microvascular anastomoses by fibrin glue. J. Surg. Sec. 45, 112–119.
15. Cikrit, D.F., Dalsing, M.C., Weinstein, T.S., Palmer, K., Lalka, S.G., and Unthank, L. (1990). CO_2-welded venous anastomosis: enhancement of weld strength with heterologous fibrin glue. Lasers Surg. Med. 10, 584–590.
16. Oz, M.C., Chuck, R.S., Johnson, J.P., Parangi, S., Bass, L.S., Nowygrod, R., and Treat, M.R. (1989). Indocyanine green dye-enhanced welding with a diode laser. Surg. Forum. 40, 316–318.
17. Chuck, R.S., Oz, M.C., Delohery, T.M., Johnson, J.P., Bass, L.S., Nowygrod, R., and Treat, M.R. (1989). Dye-enhanced laser tissue welding. Lasers Surg. Med. 9, 471–477.
18. Self, S.B., Coe, D., and Seeger, J.M. (1996). Limited throbogenicity of low temperature laser-welded vascular anstomoses. Lasers Surg. Med. 18, 241–247.
19. Tang, J., Evans, J.M., Petričević, V., Ho, P.P., and Alfano, R.R. (1999). Tissue welding using near-infrared forsterite and cunyite tunable lasers. IEEE J STQE. 5, 1103–1106.
20. Petričević, V., Gayen, S.K., and Alfano, R.R. (1988). Laser action in chromium-activated forsterite for near-infrared excitation: Is Cr^{4+} the lasing ion? Appl. Phys. Lett. 53, 2590–2592.
21. Petričević, V., Bykov, A.B., Evans, J.M., and Alfano, R.R. (1996). Room-temperature near-infrared tunable laser operation of Cr^{4+}:Ca_2GeO_4. Optic Lett. 21, 1750–1752.
22. Kopchok, G.E., White, R.A., White, G.H., Fujitani, R.M., Vlasak, J., Dykhovsky, L., and Grundfest, W.S. (1988). CO_2 argon laser vascular welding: acute histologic and thermodynamic comparison. Lasers Surg. Med. 8, 584–588.
23. Kopchok, G.E., White, R.A., Grundfest, W.S., Fujitani, R.M., Litvack, F., Klein, S.R., and White, G.H. (1988). Thermal studies of in-vivo vascular tissue fusion by argon laser. J. Invest. Surg. 1, 5–12.
24. Murray, L.W., Su, L., Kopchok, G.E., and White, R.A. (1989). Crosslinking of extracellular matrix proteins: a preliminary report on possible mechanism of argon laser welding. Lasers Surg. Med. 9, 490–496.
25. Cheong, W.F., Prahl, S.A., and Welch, A.J. (1990). A review of the optical properties of biological tissue. IEEE J. Quantum Elect. 26, 12167–12185.
26. Gayen, S.K., Zevallos, M.E., Alrubaiee, M., Evans, J.M., and Alfano, R.R. (1998). Two-dimensional near-infrared transillumination imaging of biomedical media with a chromium-doped forsterite laser. Appl. Opt. 37, 5327–5336.
27. Dixon, J.A. (1984). Lasers in surgery. Curr. Pro. Surg. XXII, 9–15.
28. Kung, R.T.V., Stewart, R.B., Zelt, D.T., L'Italien, G.J., and LaMuraglia, G.M. (1993). Absorption characteristics at 1.9 μm: effect on vascular welding. Lasers Surg. Med. 13, 12–17.
29. Marks, F.A. (1992). Optical determination of the hemoglobin oxygenation state of breast biopsies and human breast cancer xenografts in nude mice. SPIE 1641, 227–237.

Address reprint requests to:
Dr. R.R. Alfano
Institute for Ultrafast Spectroscopy and Lasers
The City College and Graduate School of the City University of New York
138th Street and Convent Avenue
New York, New York 10031

E-mail: alfano@scisun.ccny.cuny.edu